Power Quality Assessment of Voltage Positive Feedback Based Islanding Detection Algorithm

Reza Bakhshi-Jafarabadi, Reza Ghazi, and Javad Sadeh

***Abstract*—Islanding refers to a condition where distributed generators (DGs) inject power solely to the local load after electrical separation from power grid. Several islanding detection methods (IDMs) categorized into remote, active, and passive groups have been reported to detect this undesirable state. In active techniques, a disturbance is injected into the DG's controller to drift a local yardstick out of the permissible range. Although this disturbance leads to more effective detections even in well-balanced island, it raises the total harmonic distortion (THD) of the output current under the normal operation conditions. This paper analyzes the power quality aspect of the modified sliding mode controller as a new active IDM for grid-connected photovoltaic system (GCPVS) with a string inverter. Its performance is compared with the voltage positive feedback (VPF) method, a well-known active IDM. This evaluation is carried out for a 1 kWp GCPVS in MATLAB/Simulink platform by measuring the output current harmonics and THD as well as the efficiency under various penetration and disturbance levels. The output results demonstrate that since the proposed disturbance changes the amplitude of the output current, it does not generate harmonics/subharmonics. Thereby, it has a negligible adverse effect on power quality. It is finally concluded that the performance of the sliding mode-based IDM is reliable from the standpoints of islanding detection and power quality.**

***Index Terms*—Islanding detection method (IDM), power quality, sliding mode controller, total harmonic distortion (THD), voltage positive feedback (VPF).**

I. Introduction

THE penetration of renewable energy technologies increases substantially in distributed networks. In this regard, more than 80 GWp of the grid-connected photovoltaic systems (GCPVSs) have been installed worldwide in 2017, which represents a 30% growth compared to that in 2015 [1]. Although these inverter-based resources provide clean and noise-free energy to the network, they deteriorate the power quality of the available energy through the injection of current harmonics. The electrical network is susceptible to these harmonics, leading to unbalanced line voltages, variations in the voltage levels and line impedances. With respect to the considerable penetration of GCPVSs in distribution networks, the inverter's current control loop, which is responsible for DC to AC power conversion, is one of the major sources of harmonics. While this power quality degradation is negligible concerning the new switching patterns [2]-[4], active islanding detection methods (IDMs) are recently known as a new source of current harmonics [5].

Islanding is a condition in which a part of the utility including distributed generator (DG) is separated from the network, while it continues to inject power solely into the local load. This state has to be identified effectively to assure the safety of repair crew and prevent the failure of sensitive equipment [5]. Several IDMs categorized into remote and local groups have been reported in this regard [6]-[25]. Remote techniques exploit a telecommunication between DGs and upstream substation. The interconnection of DGs to the electrical network is continuously monitored through the broadcast signal and therefore, islanding can be classified in non-receiving signal circumstances [6]-[8].

As shown in Fig. 1, the measurement of the local parameters in the point of common coupling (PCC) is the basis of local techniques, including passive and active methods. When the islanding occurs, the active and reactive powers injected to or received from the public grid are stopped. Consequently, the voltage and frequency of PCC are confronted with sudden changes. These deviations or a well-defined local yardstick can be detected by passive schemes [9]-[15]. In order to reduce the none-detection zone (NDZ), i. e., the states where IDM fails to detect islanding, active algorithms are proposed [16]-[25]. In these techniques, an ongoing intentional disturbance is injected to the DG's controller to accelerate the deviation of PCC parameters in islanding events. Active frequency drift (AFD) [16], [17], impedance measurement (IM) [18]-[20], voltage positive feedback (VPF) [21]-[24], and modified sliding mode controller [25] are some examples of active schemes. Although the applied disturbance reduces the NDZ efficiently, it decreases the power quality of the output current as well. Among all power quality problems, harmonic distortion is the major concern which is quantified by total harmonic distortion (THD). The permissible ranges of the local electrical quantities are defined in IEEE Standard 1547-2008 [26] and IEC Standard 61727-2002 [27] as tabulated in Tables I and II. By this means, the inserted disturbance should be restricted to an upper limit to satisfy the power quality requirements. It is noted that in Table II, the even harmonics should be less than 25% of the odd harmonics.

Manuscript received: August 2, 2018; accepted: September 25, 2019. Date of CrossCheck: September 25, 2019. Date of online publication: January 23, 2020.

R. Bakhshi-Jafarabadi, R. Ghazi (corresponding author), and J. Sadeh are with the Electrical Engineering Department, Faculty of Engineering, Ferdowsi University of Mashhad, Mashhad, Iran (e-mail: r. bakhshi@mail. um. ac. ir; rghazi@um.ac.ir; sadeh@um.ac.ir).

DOI: 10.35833/MPCE.2018.000509

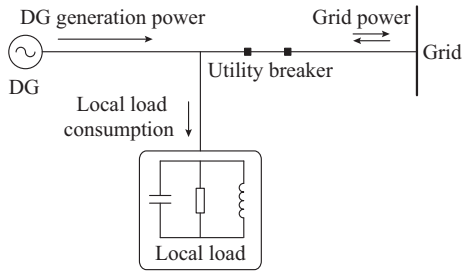

Fig. 1. Interconnection of DG and local load to electric network.

TABLE I
SUMMARY OF STANDARDS CORRESPONDING TO INTERCONNECTION OF GCPVS TO GRID

Standard	Nominal power (kW)	Maximum THD_I (%)	Voltage range (%)	Frequency range (Hz)
IEEE Standard 1547-2008	10	5	88-110	59.3-60.5
IEC Standard 61727-2002	30	5	88-110	49.0-51.0

TABLE II
DISTORTION LIMITS

Odd harmonic number (h)	Distortion limit (%)
3-9	4.0
11-15	2.0
17-21	1.5
23-33	0.6
>33	0.3

The power quality analysis of DG output power owning to the applied active IDMs has been carried out in [16]-[25], [28], [29]. Reference [16] has claimed that the ratio of the injected reactive power disturbance (ΔQ) to the active power output (P_{DG}) in AFD must be kept within the range of [–0.95%, 4.11%] to satisfy the standard requirements for a sample GCPVS. Reference [17] has developed a classic AFD technique to improve the current THD (THD_I) of a 300 Wp PV system supplying a local load. It has been remarked that the same NDZ can be attained with 30% THD_I reduction in comparison with simple AFD. A high-frequency signal injection has been presented in [18] to classify the islanded operation mode through a high-frequency IM. They recommend one inverter disturbance injection in multi DGs connection case to keep power quality in a tolerable interval. Otherwise, THD_I would be unacceptable in some multiple DGs scenarios. Reference [28] has studied the power quality assessment of ten string inverters, connected to the Brazilian power grid. The power analyzer has been employed to measure THD_I and voltage THD (THD_V) as well as power factor with a few loadings. The analysis of measured data demonstrates the compliance of the output energy with the quality requirements under a wide range of operation conditions, especially in high penetration levels. However, high THD_I and THD_V as well as low power factor have been observed at low power generations [28]. The effect of IM and AFD techniques on the power quality of a single-phase 1.5 kWp PV system has been assessed in [29]. It was argued that while THD_I rises from 0.7% to 13% in the presence of IM disturbance, its average remains acceptable (3.7%). Moreover, when the GCPVS generates low power, THD_I elevates. This occurs since the fundamental harmonic of the reference current is decreased while the disturbance size remains fixed. The power quality is not thereby satisfied in the states where GCPVS output power is less than 41.3% of its nominal value. Simulations have been developed for AFD with positive feedback (AFDPF) scheme. THD_I surpasses standard limit when the output power becomes less than 400 W (26.66% of nominal power) [29].

It can be concluded from the literature that the rate of THD_I ascent depends on the level of GCPVS output power. The current control loop is also known as the primary source of harmonics because of the disturbance injection in the frequency or angle of output current.

This paper investigates the effect of modified sliding mode controller as a new VPF-based active IDM on the output power quality of GCPVS. Since the disturbance is involved into the inverter's voltage control loop, the proposed algorithm will only change the output current amplitude rather than the frequency or angle. Consequently, its effect on the power quality of the distribution network is hardly noticeable as the same of the conventional VPF.

The rest of the paper is organized as follows. The modified sliding mode controller is introduced in Section II. In Section III, the sample of 1 kWp GCPVS case study in MATLAB/Simulink platform, including PV array and single-phase string inverter with bipolar pulse width modulation (PWM) is elaborated. Section III also presents the evaluation of the modified sliding mode controller in a few islanding scenarios and a systematic approach to define the margins of the disturbance gain. The effects of the provided disturbance on harmonics, THD_I, and efficiency as well as a comparative assessment with the classic VPF are presented in Section IV. The conclusion remarks are finally discussed in Section V.

II. DESCRIPTION OF MODIFIED SLIDING MODE CONTROLLER

VPF is an active IDM which tries to unstabilize PCC voltage after the occurrence of islanding. This aim is achieved through a VPF injection to the inverter's d-axis reference current which tunes the active power output. When the PCC voltage rises after islanding, it increases the reference current, the active power output, and consequently the PCC voltage. This voltage keeps growing in magnitude until it exceeds the over-voltage relay setting (1.1 p.u.). In the case of PCC voltage drop, the output power and voltage are diminished until the under-voltage (UV) relay setting (0.88 p.u.) is exceeded [21]-[24].

The VPF concept is employed in the sliding mode controller to represent a new active IDM [30]. In Fig. 2(a), keeping the PV current (I_{PV}) and voltage (V_{PV}) curve in mind, the locus of maximum power point (MPP) current (I_{MPP}) in the term of MPP voltage (V_{MPP}) can be estimated by a linear equation:

$$S(I_{PV}, V_{PV}) = I_{PV} - bV_{PV} + ref \tag{1}$$

where b should be determined using the least square error method and some pairs of V_{MPP} and I_{MPP} in several irradiance levels; and *ref* is an adaptive parameter that determines MPP in any climate condition. This factor should be defined in the inverter's voltage control loop using conventional MPP tracking (MPPT) techniques such as perturb and observe (P&O). In the sliding mode controller, the value of the switching surface parameter $S(I_{PV}, V_{PV})$ determines the boost converter operation condition. When $S(I_{PV},V_{PV}) > 0$, the converter switch is opened and inductor will be discharged. This increases the PV array voltage and reduces its current. On the contrary, the converter switch closes in $S(I_{PV},V_{PV}) < 0$ state, the inductor will be charged, the PV current is increaded, and the voltage is decreased. Therefore, the operation point would be regulated in such a way that the GCPVS operates around $S(I_{PV},V_{PV}) = 0$, i. e., MPP [30]. The sliding mode controller schematic diagram for GCPVS with string inverter is illustrated in Fig. 2(b), where $ref_{P\&O}$ represents the feedback effect on *ref* specified by P&O.

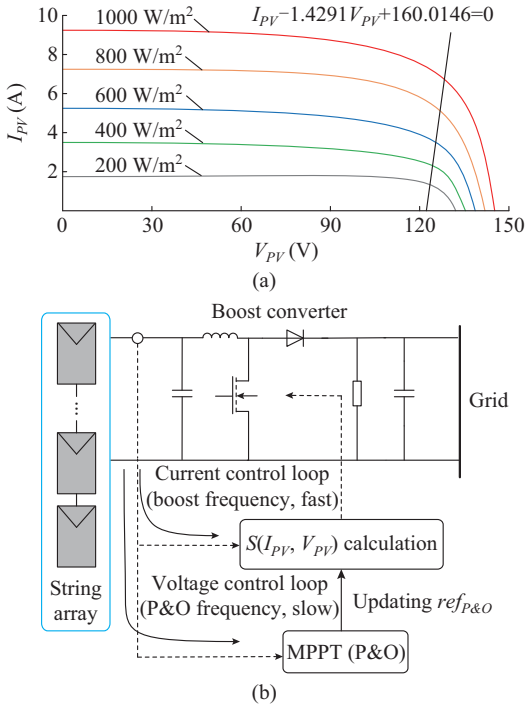

Fig. 2. Sliding mode MPPT technique. (a) Characteristics locus of V_{PV} and I_{PV}. (b) Schematic diagram.

In simple words, the basic idea of the proposed IDM is to insert a PCC voltage feedback in *ref* of the sliding mode controller as follows:

$$S(I_{PV}, V_{PV}) = I_{PV} - bV_{PV} + ref_{P\&O} - K_{pf}\Delta V_{PCC} \quad (2)$$

where K_{pf} controls the disturbance size; and ΔV_{PCC} is the PCC voltage deviation. When the grid is lost, the active power mismatch leads to a V_{PCC} variation and the applied feedback drifts *ref* away from its MPP setting. The output power is thereby reduced and will cause a voltage drop ($\Delta V_{PCC} < 0$) regarding the following equation:

$$P_{DG} = \frac{V_{PCC}^2}{R} \quad (3)$$

where R is the resistive part of the local load at PCC modeled by IEEE Standard 929-2000 [31]. For the second interval, the applied disturbance pushes *ref* more away from MPP. This reduces P_{DG} more, which results in a further V_{PCC} drop. This procedure continues until PCC voltage becomes less than 0.88 p. u. for stimulating the UV relay. In this scheme, an effective islanding classification can be achieved regarding the fast response of the sliding-mode controller in the current control loop of inverter (boost frequency, in the range of 100 kHz). The trajectory of *ref* during MPPT in grid-connected (between two isolation levels) and islanding incidents are shown in Fig. 3(a) and (b), respectively. In Fig. 3, V_{OC} and I_{SC} represent the open-circuit voltage and the short-circuit current, respectively.

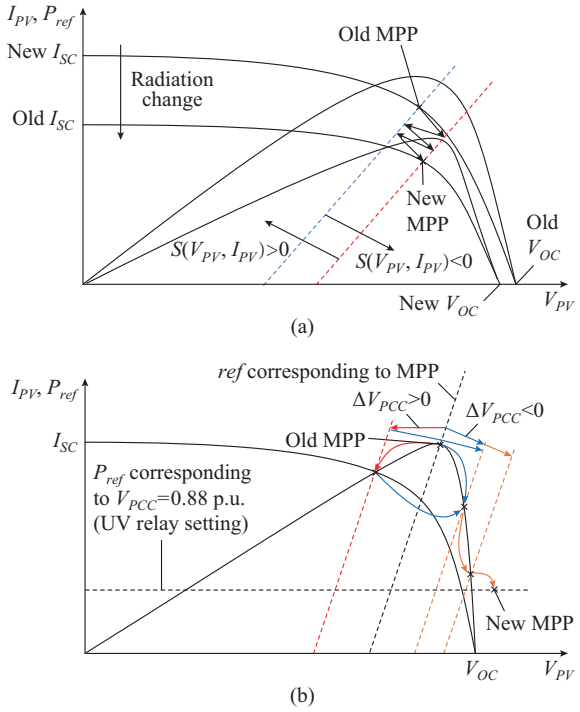

Fig. 3. Trajectory of PV array operation point in proposed method. (a) Normal operation between two irradiance levels. (b) Islanding condition.

Since the proposed disturbance is applied to the voltage control loop of inverter (MPPT) rather than the current controller, it disturbs the output current amplitude of a linear load, but not the frequency or angle. Hence, it does not generate harmonics or subharmonics, and is expected to have near-zero influence on the power quality of the distribution network.

III. Islanding Detection of Modified Sliding-mode Controller

This section contains the introduction of the case study system and justification of the modified sliding-mode controller under a few islanding scenarios. The selection criteria of the disturbance gain are detailed as well.

A. Sample System Description

The schematic of the sample system with the application

of the proposed method is shown in Fig. 4. PV array including four 250 W QPRO-G2 has been connected to the single-phase 1 kWp inverter. The parameters of this module in standard test condition (STC), i.e., 1000 W/m^2 radiation and 25 ℃ cell temperature, can be found in Table III [32]. This PV module has been simulated by single-diode model which precisely represents the module's characteristics at various uniform and non-uniform insolation levels [33]. The parameters of the current and voltage controllers of 1 kWp string inverter are tabulated in Table IV as well. It is worth mentioning that b and $ref_{P\&O}$ are 1.43 and 160.01, respectively. These settings are defined by applying some pairs of (V_{MPP}, I_{MPP}) at several insolation levels.

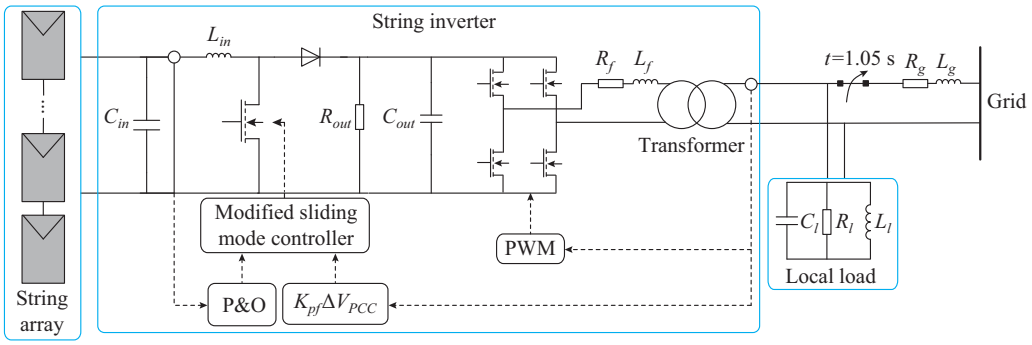

Fig. 4. Schematic of case study system under evaluation.

TABLE III
DATA OF QPRO-G2 250

Parameter	Value
Maximum power (P_{MPP})	250 W
Short-circuit current (I_{SC})	8.94 A
Open-circuit voltage (V_{OC})	37.78 V
Maximum power point current (I_{MPP})	8.45 A
Maximum power point voltage (V_{MPP})	29.89 V
Temperature coefficient of I_{SC}	3.57 mA·°C^{-1}
Temperature coefficient of V_{OC}	−124.67 mV·°C^{-1}
Temperature coefficient of P_{MPP}	−1.075 W·°C^{-1}

TABLE IV
STRING INVERTER AND TRANSFORMER PARAMETERS

Component	Parameter	Value
Boost converter	C_{in}	100 μF
	L_{in}	2 mH
	C_{out}	100 μF
	R_{out}	70 Ω
	Switching frequency	100 kHz
	P&O frequency	40 Hz
	DC link voltage	120 V
	Output voltage	250 V
String inverter	k_I	0.5
	k_P	12
	k_R	5000
	L_f	5 mH
	R_f	0.15 Ω
	PWM frequency	10 kHz
	Power factor	1.0
Transformer	Input voltage	70 V
	Output voltage	230 V
	Short-circuit impedance	0.04 p.u.

The local load is modeled as an RLC circuit with around 50 Hz resonant frequency and 2.5 quality factor Q_f to meet the islanding standard requirements (Table V) [31]. This load and GCPVS are finally integrated to the 230 V, 50 Hz single-phase network at PCC.

TABLE V
ELECTRICAL NETWORK AND LOCAL LOAD PARAMETERS

Component	Parameter	Value
Grid	L_g	100 μH
	R_g	0.012 Ω
Local load	R_l	53.98 Ω
	L_l	68.76 mH
	C_l	147.99 μF
	Q_f	2.5
	Resonant frequency	49.98 Hz

Moreover, the only setting of the proposed IDM is K_{pf}. Although the selection criteria of this parameter is described later, it is assumed to be 2.17 in the presented analysis.

It is worth mentioning that in Table IV, the input capacitance and inductance of the boost converter are denoted by C_{in} and L_{in}, while C_{out} and R_{out} represent the output capacitance and resistance, respectively. Furthermore, k_I, k_P, and k_R are the integral, proportional, and resonant gains of the inverter's current controller, respectively. They are implemented in the $\alpha\beta$ reference frame. The filter, grid, and load settings are also denoted by f, g, and l, respectively. All these parameters are shown in Fig. 4.

B. Islanding Evaluation

The modified sliding mode controller should lessen active power output, and consequently PCC voltage to reach the minimum standard setting (0.88 p.u.) for islanding classification. The islanding has been simulated for the case study system through opening the circuit breaker aside PCC in Fig. 4

at t = 1. 05 s. As mentioned above, the local load has been set to consume all generated power at STC with Q_f = 2. 5 as a worst case study and compliance with IEEE Standard 929-2000 [31].

The results including active power and PCC voltage have been illustrated in Fig. 5. In Fig. 5(a), P_L and P_G represent the active power of load and grid, respectively. The provided outputs reveal the successful push of V_{PCC} to the lower bound and precise islanding detection in less than 700 ms.

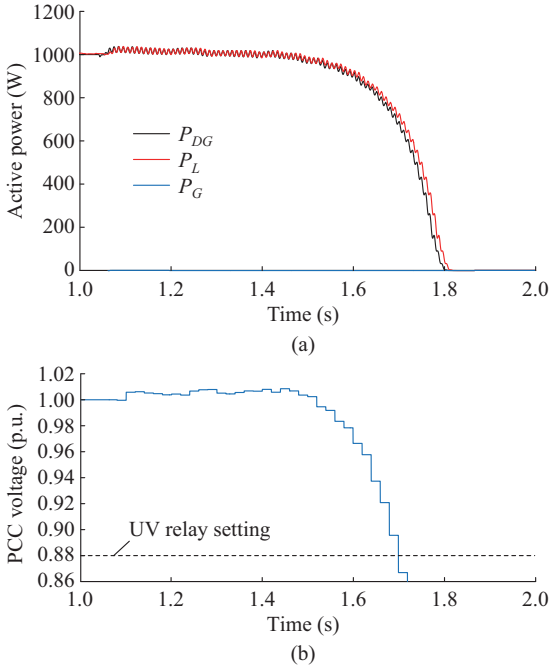

Fig. 5. Performance of proposed IDM in the worst case study. (a) Active power. (b) PCC voltage.

After islanding, the PCC voltage of the isolated region can be changed from its pre-islanding setting (V_{pr}) to a new level after separation (V_{po}) as in (4):

$$V_{po} = \frac{V_{pr}}{\sqrt{1 - \dfrac{\Delta P}{P_{DG}}}} \tag{4}$$

The post-islanding voltage depends on the active power mismatch between P_{DG} and P_L or the level of DG active power variation through activating the embedded disturbance named as active power disturbance (ΔP) [12]. While the relative active power mismatch/disturbance ($\Delta P/P_{DG}$) locates inside the range [–29.13%, 17.35%] with V_{pr} = 1 p. u., V_{po} would be inside the standard limits, i. e., 0.88 to 1.10 p. u., and islanding cannot been identified by conventional voltage relays. The study has been accordingly developed to various relative active power mismatches inside the voltage relays' blind zone and the voltage waveforms are depicted in Fig. 6. It is readily observed that the embedded disturbance successfully reduces PCC voltage to the minimum margin in all scenarios, and islanding is identified by UV relay. The provided outcomes endorse accurate islanding classification of the modified sliding-mode controller in various case studies within 700 ms.

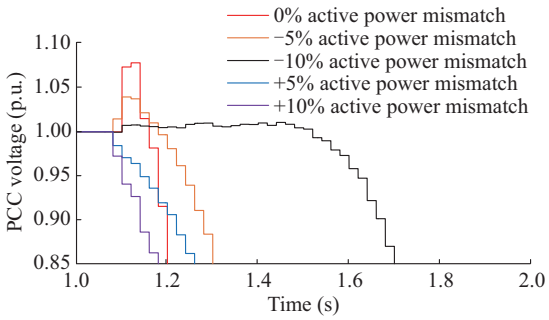

Fig. 6. PCC voltage under several active power mismatches.

C. Selection Criteria of Disturbance Size

The selection criteria of K_{pf} as the proposed disturbance gain is mandatory. The lower and upper bounds of this setting should be determined to assure the system stability in grid-connected mode and zero NDZ, respectively.

1) System stability

Disturbance gain should be limited to an upper edge to avoid unacceptable active power output reduction of the inverter under probable PCC voltage fluctuations that occur several times a day in the power system. A small signal analysis should be done to this end. By employing the modified sliding mode controller and neglecting the DC losses, the reference active power of the inverter in the voltage control loop P_{ref} can be expressed as follows:

$$P_{ref} = V_{PV}(k) I_{PV}(k) = V_{PV}(k)(S(I_{PV}, V_{PV}) + bV_{PV} - ref_{P\&O} + K_{pf}\Delta V_{PCC}) \tag{5}$$

The expressions of small signal analysis of (2) and (5) can be deduced as follows:

$$\Delta S = \Delta I_{PV} - b\Delta V_{PV} - K_{pf}\Delta V_{PCC} \tag{6}$$

$$\Delta P_{ref} = \Delta P_{PV} = V_{PV}\Delta I_{PV} + I_{PV}\Delta V_{PV} \tag{7}$$

where Δ is used to represent the small variation of current, voltage, and power around their steady-state sets. Since the variation of $ref_{P\&O}$ is near zero, the corresponding expression has been neglected in (7). When V_{PCC} decreases, the right-hand side term of (7) is positive and the GCPVS moves toward the short-circuit point. Therefore, ΔI_{PV} equals to the subtraction of the MPP current from I_{SC}. Since in both steady and transient states, the switching surface signal is zero, i.e., S = 0 and ΔS = 0, the final equation can be extracted:

$$\Delta P_{ref} = V_{PV}\Delta I_{PV} - \frac{I_{PV}K_{pf}\Delta V_{PCC}}{b} \tag{8}$$

This expression is deduced by supposing that ΔI_{PV} is proportionally smaller in comparison with other terms. Equation (8) can be used to calculate the reference active power variation with a given PCC voltage change by approaching the time reference in the positive neighborhood of zero ($\Delta t \rightarrow 0^+$). This reference power is equal to P_{DG} by neglecting the losses of the DC/AC conversion process.

The mentioned analysis cannot be applied in the case of $\Delta V_{PCC} > 0$ since $-K_{pf}\Delta V_{PCC}$ would be negative and the GCPVS moves toward the open-circuit point. The final lev-

els of I_{PV} and ΔI_{PV} would be unknown in this situation, and ultimately, the first term in (8) could not be defined.

This expression, however, can be employed to determine the upper bound for a maximum acceptable P_{DG} reduction and a given step voltage size for $\Delta V_{PCC} < 0$. For instance, by assuming 0.03 p.u. and 10% as the PCC voltage variation and maximum permissible fluctuations for P_{DG}, respectively, the computational results (only for $\Delta V_{PCC} < 0$ case) as well as the simulation outcomes are provided in Table VI. Based on these findings, K_{pf} should be restricted to 3.04 to assure at most 10% P_{DG} drop with 3% V_{PCC} change.

TABLE VI
P_{DG} REDUCTION IN RESPONSE TO A 3% V_{PCC} CHANGE

K_{pf}	Voltage fall (%)		Voltage rise in simulation (%)
	Simulation	Calculation	
2.17	3.97	3.53	8.99
3.04	7.90	6.56	10.11
4.35	12.56	11.80	24.28

2) Zero non-detection zone

The lower margin of K_{pf} can be defined respecting the successful detection in worst islanding scenario, i.e., zero active power mismatch or disturbance. As mentioned above, while the relative active power disturbance locates inside the range of [–29.13%, 17.35%], V_{po} would not leave the standard range. Accordingly, if the proposed IDM diminishes P_{DG} by 29.13 in zero active power mismatch, the PCC voltage would be successfully drifted to the lower margin (0.88 p.u.), and the islanding is identified.

Equation (5) can also be manipulated to (9) concerning the fact that $S(I_{PV}, V_{PV}) + bV_{PV} - ref_{P\&O}$ equals to zero in all operation modes:

$$P_{DG} + \Delta P = P_{ref} = V_{PV} K_{pf} \Delta V_{PCC} \tag{9}$$

This equation can be further simplified by replacing V_{PV} using (2) and neglecting I_{PV} against $ref_{P\&O}$:

$$P_{DG} + \Delta P = \frac{ref_{P\&O} - K_{pf} \Delta V_{PCC}}{b} K_{pf} \Delta V_{PCC} \tag{10}$$

The following polynomial term can be finally derived to determine the upper limit of K_{pf} with a given PCC voltage variation:

$$(K_{pf} \Delta V_{PCC})^2 - ref_{P\&O} K_{pf} \Delta V_{PCC} + b(P_{DG} + \Delta P) = 0 \tag{11}$$

The right-hand side term can be negative or positive regarding the level of (P_{DG} + ΔP). However, since the signs of the first and second terms are different, this equation has at least one positive solution. For instance, in order to assure islanding classification of the case study system with zero NDZ with ΔV_{PCC} = 0.002 p.u. (460 mV) and ΔP = 29.13%, K_{pf} should be at least 1.53 while voltage samples are measured in p.u.

Therefore, the optimized K_{pf} range for the case study GCPVS is [1.53, 3.04]. This range is defined self-standing regardless of the DG, inverter, and grid characteristics.

The same criteria have been considered for the definition of the VPF disturbance size and limited to the range of [17.80, 25.05] for case study system [21]-[24].

The effect of VPF and the proposed modified sliding-mode controller on power quality is assessed in the next section for the prototype system. In the following simulations, the disturbance gain is selected to be 20 and 2.17 for VPF and modified sliding mode controller. These selections guarantee zero NDZ and stable performance of the studied GCPVS in normal operation conditions.

IV. POWER QUALITY ASSESSMENT

The performance and efficiency of the sliding-mode-based IDM in the standpoints of current harmonics THD_I are studied. The efficiency has not been placed in the power quality factors in scientific sources [34]. However, since the proposed IDM deviates GCPVS operation point away from MPP, the variation of efficiency is assessed as well.

A. THD

The presence of harmonics in the electrical system deviates voltage or current from its original sinusoidal waveforms. This deviation can be measured by THD, defined as the ratio of the root-mean-square (RMS) voltage or current of the harmonics to the fundamental component. Based on IEEE Standard 1547-2008 and IEC Standard 61727-2002, THD_I should be limited to 5%. Furthermore, harmonic components should be restricted to the values listed in Table II [26], [27].

The analysis is initially performed at various active power production levels. The results, including THD_I for classic VPF and modified sliding-mode IDM are presented in Fig. 7.

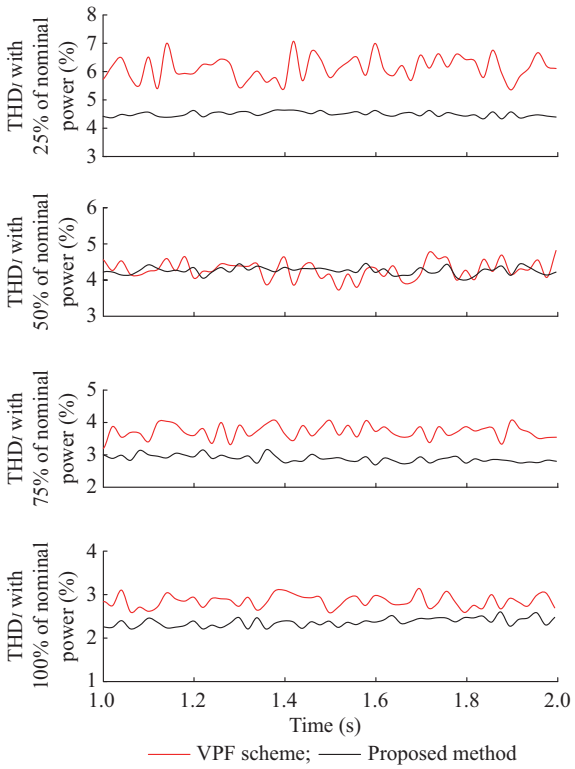

Fig. 7. Effect of VPF and proposed schemes on THD_I with different percentages of nominal power.

In addition, the harmonic spectra (for $h < 20$) in 25% of STC output power are illustrated in Fig. 8. It can be seen that, unlike VPF, THD_I and the harmonic components are acceptable in the presence of the disturbance in the modified sliding-mode approach. When the amplitude of the output current (power) is decreased, THD_I in VPF is raised due to a fixed disturbance size. On the contrary, the disturbance size of sliding-mode IDM is controlled in the voltage control loop (MPPT) taking into account the DG's active power output. Therefore, it can provide low THD_I even in low power generation. The minimum output power level of sample GCPVS for classic VPF with acceptable power quality is 285 W while it is 195 W for the proposed IDM. This highlights the wider operation range of the GCPVS with acceptable power quality when it is equipped with the proposed scheme.

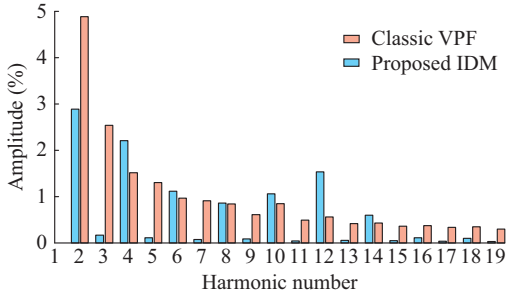

Fig. 8. Effect of classic VPF and proposed IDM on power quality (harmonic spectra).

The disturbance size and amount of generated power are critical variables in power quality analysis of the active IDMs. In this regard, the average THD_I at a few disturbance and generation levels has been determined and depicted in Fig. 9. Figure 9 shows that THD_I is within the standard limits in the proposed IDM for a given disturbance size regardless of the output power levels. However, K_{pf} has to be restricted in VPF scheme to satisfy the standards in the low output power rate. Furthermore, Fig. 9(a) confirms that the proposed disturbance provides smaller adverse effect on THD_I at the same level of output power.

The commercial and power plant GCPVSs can be formed by string inverters, where multi-inverters are connected to the same PCC. The effect of multi-identical GCPVSs connection on the THD_I has been assessed in this part. Table VII shows the average THD_I of multi-DGs connection in 25% of nominal power. The outcomes imply on the acceptable power quality of the presented algorithm with multi-GCPVSs.

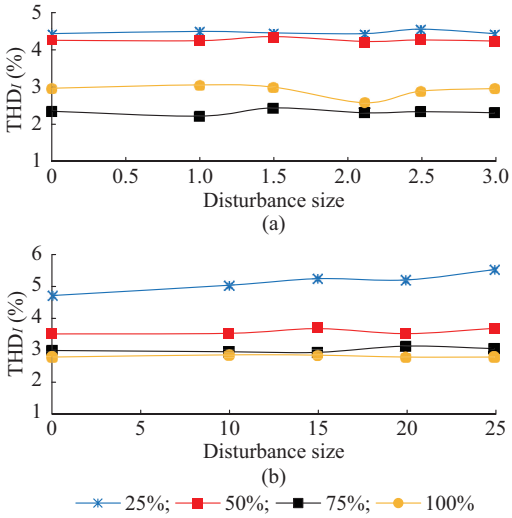

Fig. 9. Average THD_I for different disturbance sizes. (a) Modified sliding mode. (b) Classic VPF.

TABLE VII
AVERAGE THD_I IN MULTI-DGS CONNECTION OF LOW POWER GENERATION SCENARIO

GCPVS no.	THD_I (%)
1	4.49
2	4.40
3	4.47
4	4.65
5	4.53

B. Efficiency

The average MPPT efficiency, i.e., the ratio of DC link power to the PV array power as well as the inverter efficiency, i.e., the ratio of AC output active power to the PV array power, for the sample GCPVS equipped with the proposed algorithm at various irradiance levels have been measured. What can be inferred from the provided data in Table VIII is that the presented disturbance has little influence on the DG's efficiency, since MPP can be accomplished at a small bound around *ref* as the same as other MPPT algorithms. Hence, besides effective islanding detection, a high efficiency is guaranteed in normal operational mode. In addition, since the disturbance of VPF algorithm has been employed in the current controller of the inverter, it does not change the MPPT operation and efficiency.

TABLE VIII
EFFECT OF SUGGESTED DISTURBANCE ON MPPT AND INVERTER EFFICIENCIES

Radiation (W/m^2)	MPPT efficiency with proposed method (%)	MPPT efficiency without proposed method (%)	Inverter efficiency with proposed method (%)	Inverter efficiency without proposed method (%)
250	98.18	98.21	98.07	98.04
500	96.18	96.27	96.12	96.22
750	95.96	96.00	95.96	95.98
1000	96.05	96.05	96.04	96.04

V. Conclusion

In this paper, the influence of the classic VPF and modified sliding-mode IDM on the GCPVS's power quality and efficiency has been evaluated. The study has been done for a 1 kWp PV system with string inverter. The simulation results show that, while the THD of output current in the proposed IDM is smaller than the simple VPF, both methods render acceptable power quality in a wide range of system operation. This proper performance has been achieved due to the variation of the current magnitude rather than the angle or frequency. This magnitude variation is realized in VPF and the proposed method in the current and voltage control loops (MPPT), respectively. The simulations also confirm that the acceptable THD_I and harmonics are guaranteed in multi-GCPVSs connection situation even at low power generation levels as the worst scenario.

Since the new technique tries to deviate the system from its MPP condition, the effect of embedded disturbance on the efficiency is also performed. In this regard, the simulations are carried out and a negligible reduction in MPPT and inverter efficiencies (less than 0.04%) has been demonstrated in the proposed method. This occurs since MPP can be gained at a small bound around *ref*.

It has been finally concluded that the modified sliding-mode controller has the advantages of the conventional VPF scheme in islanding detection as well as a higher power quality in the production of energy.

References

[1] A. Jäger-Waldau, "PV status report 2017," Publications Office of the European Union, Luxembourg, 2018.

[2] M. Sandhu and T. Thakur, "Harmonic minimization in a modified cascaded multilevel inverter for islanded microgrid using two switching techniques," *International Journal of Grid and Distributed Computing*, vol. 10, no. 12, pp. 11-20, Dec. 2017.

[3] S. Natarajan and R. S. R. Babu, "Reduction of total harmonic distortion in cascaded H-bridge inverter by pattern search technique," *International Journal of Electrical and Computer Engineering (IJECE)*, vol. 7, no. 6, p. 3292, Dec. 2017.

[4] A. Luo, Q. Xu, F. Ma *et al.*, "Overview of power quality analysis and control technology for the smart grid," *Journal of Modern Power Systems and Clean Energy*, vol. 4, no. 1, pp. 1-9, Jan. 2016.

[5] A. Khamis, H. Shareef, E. Bizkevelci *et al.*, "A review of islanding detection techniques for renewable distributed generation systems," *Renewable and Sustainable Energy Reviews*, vol. 28, pp. 483-493, Dec. 2013.

[6] W. Xu, G. Zhang, C. Li *et al.*, "A power line signaling based technique for anti-islanding protection of distributed generators – part I: scheme and analysis," *IEEE Transactions on Power Delivery*, vol. 22, no. 3, pp. 1758-1766, Jul. 2007.

[7] G. Bayrak, "A remote islanding detection and control strategy for photovoltaic-based distributed generation systems," *Energy Conversion and Management*, vol. 96, pp. 228-241, May 2015.

[8] G. Bayrak and E. Kabalci, "Implementation of a new remote islanding detection method for wind-solar hybrid power plants," *Renewable and Sustainable Energy Reviews*, vol. 58, pp. 1-15, May 2016.

[9] J. C. M. Vieira, D. S. Correa, W. Freitas *et al.*, "Performance curves of voltage relays for islanding detection of distributed generators," *IEEE Transactions on Power Systems*, vol. 20, no. 3, pp. 1660-1662, Aug. 2005.

[10] J. C. M. Vieira, W. Freitas, W. Xu *et al.*, "Performance of frequency relays for distributed generation protection," *IEEE Transactions on Power Delivery*, vol. 21, no. 3, pp. 1120-1127, Jul. 2006.

[11] Y. Shang, S. Shi, and X. Dong, "Islanding detection based on asymmetric tripping of feeder circuit breaker in ungrounded power distribution system," *Journal of Modern Power Systems and Clean Energy*, vol. 3, no. 4, pp. 526-532, Oct. 2015.

[12] E. Kamyab and J. Sadeh, "Islanding detection method for photovoltaic distributed generation based on voltage drifting," *IET Generation, Transmission & Distribution*, vol. 7, no. 6, pp. 584-592, Jun. 2013.

[13] M. Bakhshi, R. Noroozian, and G. B. Gharehpetian, "Islanding detection scheme based on adaptive identifier signal estimation method," *ISA Transactions*, vol. 71, pp. 328-340, Nov. 2017.

[14] M. Mishra, M. Sahani, and P. K. Rout, "An islanding detection algorithm for distributed generation based on Hilbert-Huang transform and extreme learning machine," *Sustainable Energy, Grids and Networks*, vol. 9, pp. 13-26, Mar. 2017.

[15] P. P. Das and S. Chattopadhyay, "A voltage-independent islanding detection method and low-voltage ride through of a two-stage PV inverter," *IEEE Transactions on Industry Applications*, vol. 54, no. 3, pp. 2773-2783, May 2018.

[16] L. A. C. Lopes and H. Sun, "Performance assessment of active frequency drifting islanding detection methods," *IEEE Transactions on Energy Conversion*, vol. 21, no. 1, pp. 171-180, Mar. 2006.

[17] A. Yafaoui, B. Wu, and S. Kouro, "Improved active frequency drift anti-islanding detection method for grid connected photovoltaic systems," *IEEE Transactions on Power Electronics*, vol. 27, no. 5, pp. 2367-2375, May 2012.

[18] D. Reigosa, F. Briz, C. B. Charro *et al.*, "Active islanding detection using high-frequency signal injection," *IEEE Transactions on Industry Applications*, vol. 48, no. 5, pp. 1588-1597, Sep. 2012.

[19] T. Bei, "Accurate active islanding detection method for grid-tied inverters in distributed generation," *IET Renewable Power Generation*, vol. 11, no. 13, pp. 1633-1639, Nov. 2017.

[20] H. F. Xiao, Z. Fang, D. Xu *et al.*, "Anti-islanding protection relay for medium voltage feeder with multiple distributed generators," *IEEE Transactions on Industrial Electronics*, vol. 64, no. 10, pp. 7874-7885, Oct. 2017.

[21] P. Du, Z. Ye, E. E. Aponte *et al.*, "Positive-feedback-based active anti-islanding schemes for inverter-based distributed generators: basic principle, design guideline and performance analysis," *IEEE Transactions on Power Electronics*, vol. 25, no. 12, pp. 2941-2948, Dec. 2010.

[22] S. K. Kim, J. H. Jeon, H. K. Choi *et al.*, "Voltage shift acceleration control for anti-islanding of distributed generation inverters," *IEEE Transactions on Power Delivery*, vol. 26, no. 4, pp. 2223-2234, Oct. 2011.

[23] F. J. Lin, J. H. Chiu, Y. R. Chang *et al.*, "Active islanding detection method using *d*-axis disturbance signal injection with intelligent control," *IET Generation, Transmission & Distribution*, vol. 7, no. 5, pp. 537-550, May 2013.

[24] A. Samui and S. R. Samantaray, "An active islanding detection scheme for inverter-based DG with frequency dependent ZIP-exponential static load model," *International Journal of Electrical Power & Energy Systems*, vol. 78, pp. 41-50, Jun. 2016.

[25] R. Bakhshi and J. Sadeh, "Voltage positive feedback based active method for islanding detection of photovoltaic system with string inverter using sliding mode controller," *Solar Energy*, vol. 137, pp. 564-577, Nov. 2016.

[26] *IEEE Standard for Interconnecting Distributed Resources with Electric Power Systems*, IEEE Standard 1547-2008, 2008.

[27] *Characteristics of the Utility Interface for Photovoltaic (PV) Systems*, IEC 61727, 2002.

[28] G. A. Rampinelli, F. P. Gasparin, A. J. Bühler *et al.*, "Assessment and mathematical modeling of energy quality parameters of grid connected photovoltaic inverters," *Renewable and Sustainable Energy Reviews*, vol. 52, pp. 133-141, Dec. 2015.

[29] M. Hamzeh and H. Mokhtari, "Power quality comparison of active islanding detection methods in a single phase PV grid connected inverter," In *Proceedings of IEEE International Symposium on Industrial Electronics (ISIE 2009)*, Seoul Olympic Parktel, Korea, Jul. 2009, pp. 1-6.

[30] Y. Levron and D. Shmilovitz, "Maximum power point tracking employing sliding mode control," *IEEE Transactions on Circuits and Systems I: Regular Papers*, vol. 60, no. 3, pp. 724-732, Mar. 2013.

[31] *IEEE Recommended Practice for Utility Interface of Photovoltaic (PV) Systems*, IEEE Standard 929-2000, 2000.

[32] Q CELLS Official Website. (2018, Aug.). QPRO-G2 data. [Online]. Available: www.q-cells.com

[33] K. Ding, X. Bian, H. Liu *et al.*, "A MATLAB-Simulink-based PV module model and its application under conditions of nonuniform irradiance," *IEEE Transactions on Energy Conversion*, vol. 27, no. 4, pp. 864-872, Dec. 2012.

[34] R. C. Dugan, M. F. McGranaghan, S. Santoso *et al.*, *Electrical Power Systems Quality*, 3rd ed. New York: McGraw-Hill, 2003.

Reza Bakhshi-Jafarabadi received the B.Sc. and M.Sc. degrees in electrical engineering from Ferdowsi University of Mashhad, Mashhad, Iran, in 2011 and 2014, respectively. He is currently a Ph.D. student at Department of Electrical Engineering, Ferdowsi University of Mashhad. His research interests include renewable energy technologies and integration of distributed generators into the power system.

Reza Ghazi received his B.Sc. degree (with honours) from Tehran University of Science and Technology, Tehran, Iran, in 1976. In 1986, he received his M.Sc. degree from Manchester University, Institute of Science and Technology (UMIST), Manchester, UK, and the Ph.D. degree in 1989 from the University of Salford, Manchester, UK, all in electrical engineering. Following receipt of the Ph.D degree, he joined the faculty of engineering Ferdowsi University of Mashhad, Mashhad, Iran as an Assistant Professor of electrical engineering. He is now Professor of electrical engineering in Ferdowsi University of Mashhad. He has published over 100 papers in these fields including three books. His main research interests are reactive power control, FACTS devices, application of power electronic in power systems, distributed generation, restructured power systems control and analysis.

Javad Sadeh received the B.Sc. and M.Sc. degrees in electrical engineering (with honours) from Ferdowsi University of Mashhad, Mashhad, Iran, in 1990 and 1994, respectively, and the Ph.D. degree in electrical engineering from Sharif University of Technology, Tehran, Iran, with the collaboration of the electrical engineering laboratory of the Institut National Polytechnique de Grenoble (INPG), Grenoble, France, in 2001. Currently, he is Professor in the Department of Electrical Engineering, Ferdowsi University of Mashhad. He is also educational office manager of Ferdowsi University of Mashhad. His research interests are power system protection, dynamics, operation as well as renewable energy technologies.